Desalination and Water Treatment
www.deswater.com

doi:10.5004/dwt.2019.23646

148 (2019) 30–41
April

Simulation of heat and mass transport for ethylene glycol solution separation using a vacuum membrane distillation process

Sahar Abdolbaghi[a], Hamid Reza Mahdavi[b], Toraj Mohammadi[b,*]

[a]*Faculty of Chemical Engineering, Islamic Azad University, South Tehran Branch, Tehran, Iran, Tel. +98 21 77240051, Fax +98 21 77240051, email: sahar_abdolbaghi@yahoo.com (S. Abdolbaghi)*
[b]*Research and Technology Centre of Membrane Processes, Faculty of Chemical Engineering, Iran University of Science and Technology (IUST), Narmak, Tehran, Iran, Tel. +98 21 77240051, Fax +98 21 77240051, email: hamidreza_mahdavi@chemeng.iust.ac.ir (H.R. Mahdavi), Tel. +98 21 77240051, Fax +98 21 77240051, email: torajmohammadi@iust.ac.ir (T. Mohammadi)*

Received 14 February 2018; Accepted 20 December 2018

ABSTRACT

In this research, a comprehensive model was extended to study the effects of different vacuum membrane distillation (VMD) parameters in flat membrane modules. The model is based on computational fluid dynamics (CFD) which uses the finite element method (FEM) as a powerful tool to solve different partial differential equations (PDEs) simultaneously. COMSOL Multiphysics as a commonly used software for problems involving Navier–Stokes and mass conservation equations based on FEM, was used. Furthermore, the fugacity coefficient was used in order to calculate vapor and liquid activity coefficients. Vacuum membrane distillation was used as a separation method for ethylene glycol (EG) solution separation using a flat polypropylene (PP) membrane module. Flow distribution through the membrane was obtained by two mass transfer mechanisms; Knudsen and free diffusion. Furthermore, the calculated vapor pressure using the UNIQUAC method was used as a reference vapor pressure. Effects of operating parameters comprising feed temperature, feed concentration and vacuum pressure and effects of membrane characteristics including porosity, pore size and thickness on permeate flux were investigated. Moreover, field distributions (velocity, temperature and concentration) and flux along the membrane module were studied. Based on results, increasing feed temperature, porosity and pore size leads to permeate flux enhancement, while increasing vacuum pressure, feed concentration and thickness causes to permeate flux diminution. Furthermore, the simulation validation was performed using the comparison of results with the experimental data. Hence, the model was found to have significant potential for simulating VMD involving different aqueous solutions.

Keywords: Vacuum membrane distillation; Computational fluid dynamics; Finite element method; COMSOL multiphysics; Ethylene glycol solution separation

1. Introduction

Ethylene glycol (EG) is a dihydroxy alcohol and it is well known because of its high boiling point (197.6°C) and freezing point well below zero (–13°C). According to these properties, EG can be used in most of the commercial coolant liquids, in airports as deicer liquid and in other industries like pharmaceutical as surface active agents, plastic and plasticizers [1]. Production of EG in Canada, Germany, United States of America and other countries is abundant so there are large amounts of EG in wastewaters. It is chemically harmful and as a result, direct discharge of EG into sewage is not allowed in many countries because aquatic organisms are exposed to high concentrations of EG [1,2]. In this case, wastewater treatment by incineration is not recommended because of the high amount of water, there-

*Corresponding author.

fore EG recovery seems to be the best solution. For protecting the aquatic and terrestrial organisms from EG toxicity effects, chemical and/or physical treatment can be used [2].

Water is the crucial matter in human's life. Deficiency of water cloud is an important problem in the future, especially in tropical regions. Because of the increasing global population, the world may be faced with great fresh water scarcity [3]. Water resources are limited; therefore, water treatment is the only alternative way to obtain fresh water in coming decades. Thus, wastewater treatment techniques which are suitable, rapid and inexpensive are the essential requirements of the present century [4]. There are different techniques such as coagulation, precipitation, oxidation, crystallization, evaporation, adsorption, distillation, electrodialysis, ion exchange, solvent extraction and membrane filtration applied for water treatment [5].

Nowadays, membrane separation processes are utilized in important industrial operations with significant technical and commercial impact unlike the past when they had only simple applications in laboratories [6–8]. The membrane processes with pressure separation processes driven are microfiltration [9], ultrafiltration [10], reverse osmosis and nanofiltration [11]. Membrane processes with concentration gradient driving force are vapor permeation, gas separation, liquid membrane and dialysis. Finally, thermally driven separation processes are diffusion osmosis and membrane distillation (MD) [3,5,6].

Membrane distillation is one of the separation methods usually used for the preparation of pure water. Hydrophobic membranes are used in this method [12]. This method is a thermally driven separation process that only vapor can be transferred through membrane [13,14]. In fact, the vapor pressure gradient between the membrane surfaces resulted in occurring of separation process [15]. Membrane distillation can be operated at atmospheric pressure and low temperature. This process can be an alternative to conventional separation processes like distillation and reverse osmosis due to low cost and energy saving [16]. Furthermore, its relating process equipment is much smaller in comparison to conventional distillation which relies on high vapor velocities to provide cordial vapor-liquid contact. It's due to using a hydrophobic microporous membrane. Furthermore, the required operating temperature is much lower because there is no need for the high heat process liquids with high boiling temperatures [14]. Thus, it's needed energy can be supplied using solar energy or waste heat from industrial facilities [17,18]. However, this method is not yet on the industrialization stage because of providing lower flux than existing industrial methods [19].

There are four different MD configurations to induce vapor pressure gradients across the membranes, including sweeping gas membrane distillation (SGMD), air gap membrane distillation (AGMD), direct contact membrane distillation (DCMD) and vacuum membrane distillation (VMD) [14,20]. In VMD configuration, a vacuum pump is used to provide a vacuum in the permeate side and a condenser is used to condensate permeate outside of the membrane module [15,21]. Applying vacuum resulted in obtaining the vapor pressure gradient across the membrane pores. Thus, water vapor can be drawn towards the permeate side quickly through the membrane pores [22]. This greatly increases the vapor transfer by Poiseuille flow and/or Knudsen diffusion [23]. Moreover, because of the rapid removal of water vapor in the permeate side, the boundary layer of mass transfer is mitigated effectively. Thus, with the both mentioned effects, VMD is going to have higher permeate flux and totally VMD displays the advantages of higher permeate flux and better thermal efficiency compared with other MD processes [23–25].

To improve the performance of the VMD process, it is necessary to spend money and time on research and simulation. Furthermore, appropriate mathematical models can be applied as another alternative method. One of the useful and powerful tools for modeling of the process is computational fluid dynamics (CFD). Problems involving mass transfer, heat transfer, fluid flow can be effectively solved using CFD, which has been widely used in membrane separation process simulations [26]. Compartment models for predictive scale-up of processes have been recently developed using CFD simulations [27]. Computational fluid dynamics has a glorious history, but its popularity increased in the late 1990s for modeling different transport phenomena [28]. Since then it was used as an efficient tool in order to model different geometries in a steady state or unsteady state modes [29].

Different approaches were used by several researchers to model the VMD process. Soni et al. implemented universal quasi-chemical functional group activity coefficients (UNIFAC) to determine vapor pressures in the membrane-liquid interface for aromatic hydrocarbons separation in flat modules [30]. Diban et al. proposed that Knudsen diffusion and free diffusion both mass transfer mechanisms can involve transport in the membrane. They also used the UNIFAC method in their thermodynamic modeling [31]. Hayer et al. developed a model to study the parameters involved in VMD using COMSOL Multiphysics. Their model involved simultaneous simulation of heat transfer, mass transfer and fluid flow [32]. Lovineh et al. investigated the effects of operating parameters in VMD for desalination of Persian Gulf water by solving numerically model via MATLAB. Influences of some operating conditions on permeate flux such as feed temperature, feed concentration and vacuum pressure as well as some membrane characteristics such as porosity, thickness and pore size were considered [33]. Although simulation of VMD was investigated in different researches, using two volatile liquids as feed solution such as water and EG has been rarely reported in the articles.

In this research, a comprehensive model was extended to study VMD simulation of water extraction from EG solution as a volatile material using a flat PP membrane. The model is based on CFD which uses the Finite Element Method (FEM). Computational fluid dynamics was the method used to solve PDEs numerically. Finite element method which is a common discretization method in CFD was found to be a convenient method to solve coupled heat, mass and Navier-Stokes PDEs. Furthermore, the fugacity coefficient was used in order to calculate vapor and liquid activity coefficients. To ensure accuracy of the results, the calculated vapor pressure by Raoul's law were compared with the predicted values by the HYSYS software. Moreover, the effects of operating parameters comprising feed temperature, feed concentration and vacuum pressure and effects of membrane characteristics including porosity, pore size and thickness on permeate flux were investi-

gated. Moreover, field distributions (velocity, temperature and concentration) and flux along the membrane module were studied. Flow distribution through the membrane was obtained by two mass transfer mechanisms; Knudsen and free diffusion. Furthermore, the calculated vapor pressure using the UNIQUAC method was used as a reference vapor pressure. Furthermore, the simulation validation was carried out to investigate the simulation accuracy.

2. Methodology

A two-dimensional comprehensive model has been used for VMD simulation in order to investigate momentum, heat and mass transfer. Heat, momentum and mass transfer were evaluated simultaneously with consideration of their interaction with each other. The algorithms of coupling were solved in COMSOL Multiphysics. For this purpose, the operating variables and membrane characteristics were presented in Table 1 [2,34]. Due to membrane hydrophobic characteristic, a non-wetted approach was assumed for numerical simulation of the flat module. This approach indicates that the water entering into the membrane pores is inconsiderable. It was assumed a vapor and liquid thermodynamic equilibrium condition in the membrane–feed and membrane–permeate interfaces. Additionally, the following assumptions were considered for this modeling [32]:

- The conditions are steady-state
- No transmembrane flow of EG (100% rejection)
- No slip condition on the membrane-liquid surface
- Effect of feed pressure on vapor pressure is negligible
- Mass transfer is not consider in feed side (Due to the negligible amount of steam removal compared to the feed amount, it can be concluded that there is not useful considering mass transfer in the feed side. Consequently, it can be supposed that there is no effect of mass transfer in the feed side.)
- Darcy velocity is not considered due to its low value (Darcy and Knudsen mechanisms are used for fluid flow transport. Darcy mechanisms is dominant when pore size is large enough whereas Knudsen mechanism is dominant when pore size is small enough. Thus, in this simulation due to small pore size, Knudsen mechanism is significant and Darcy mechanism is not considerable).

Table 1
Operating variables[2,34]

Variables	Value
Vacuum pressure, Pa	0.3
Feed velocity, m s^{-1}	0.003
Membrane porosity, %	75
Membrane tortuosity	2.25
Membrane pore size, μm	0.2
Membrane thickness, μm	165
Inlet temperature, °C	40–80
Solution concentration, wt. %	20–60
Module dimension, cm^2	4*10

2.1. Model equations

As indicated in Fig. 1, the simulation cell as a two-dimensional approach was comprised of three subdomains (feed, membrane and permeate).Furthermore, the dimensions were unified using the dimensionless length which is defined as the ratio of the length to the total module length.

2.1.1. Fluid flow in feed and permeate subdomains

In order to evaluate momentum transfer in the feed and the permeate sides, continuity equation [Eq. (1)] and Navier–Stokes equation [Eq. (2)] should be solved in both subdomains simultaneously [35].

$$\nabla\cdot(\rho u)=0 \tag{1}$$

$$-\mu\Delta u+\rho(u\cdot\nabla)u+\rho\nabla p=0 \tag{2}$$

where ρ is density (kg m^{-3}), u demonstrates velocity vector (m s^{-1}), p indicates pressure (Pa) and μ represents dynamic viscosity (Pa·s). In this research, effects of feed and permeate flows on transmembrane flux were considered. Furthermore, the diffusive and convective fluxes contributions were noticed. Inlet velocity into the permeate side was determined by Eq. (3) [36].

$$u=\frac{\left(\frac{\partial C_{mem.vapor}}{\partial y}\right)D_{eff}M_w}{\rho_v} \tag{3}$$

where $C_{mem.vapor}$, D_{eff}, M_w and ρ_v present vapor concentration on membrane side (mol m^{-3}), effective diffusion coefficient (m^2 s^{-1}), water molecular weight (kg mol^{-1}) and vapor density (kg m^{-3}), respectively.

The above equation was derived using mass balance. Table 3 and Table 4 describe boundary conditions for each subdomain in detail.

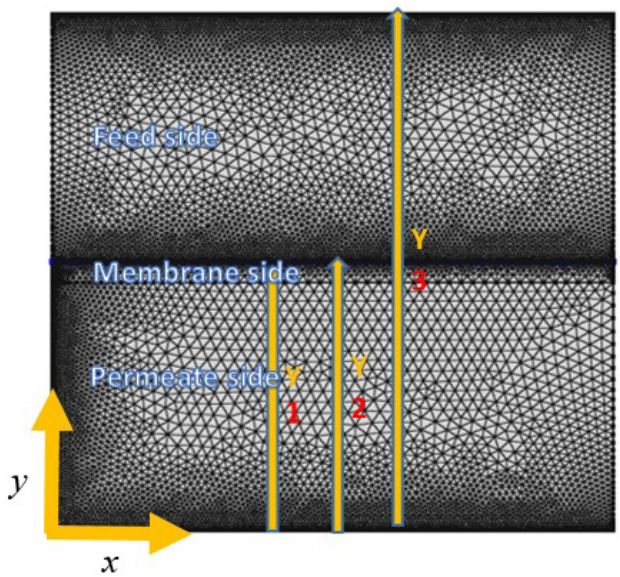

Fig. 1. Triangular mesh used in VMD simulation.

2.1.2. Mass transfer in membrane subdomain

In this research, simultaneous effect of diffusive and convective mechanisms on mass transfer was considered. The basic diffusion is defined by diffusive mechanism, which is affected by Knudsen diffusion model in porous media. Therefore, in the definition of diffusive flux, both Fick's diffusion and Knudsen diffusion mechanisms are contributed [37]. It was supposed that all of the air molecules had been already washed away from pores and the vacant space in the membrane is only filled with substances present in the feed. As mentioned, mass transfer is not considered in feed side. There are many equations to obtain the gases diffusion coefficient. One of their most basic is Wilke-Lee equation as presented by Eq. (4) [36].

$$D_{AB}=\frac{10^{-4}\left(1.084-0.249\sqrt{\frac{1}{M_A}+\frac{1}{M_B}}\right)T^{\frac{3}{2}}\sqrt{\frac{1}{M_A}+\frac{1}{M_B}}}{p_t\left(r_{AB}\right)^2 f\left(\frac{k\cdot T}{\varepsilon'_{AB}}\right)} \tag{4}$$

in which D_{AB}, T, M_A, M_B, P_t, r_{AB}, ε'_{AB}, k' and f ($k'T\,\varepsilon'^{-1}_{AB}$) are diffusion coefficient ($m^2\ s^{-1}$), temperature (K), molecular weight of A (kg k mol^{-1}), molecular weight of B (kg k mol^{-1}), absolute pressure (N m^{-2}), collision diameter (nm), energy of molecular attraction (J), Boltzmann constant (J K^{-1}) and collision function, respectively. In order to calculate r and ε′, Eqs. (5) and Eq. (6) were used, respectively [32].

$$r=1.18v^{1/3} \tag{5}$$

$$\frac{\varepsilon'}{k'}=1.21T_b \tag{6}$$

where ν is molecular volume ($m^3\ mol^{-1}$), T_b is the boiling point (K) and collision function can be calculated by available charts. Mass transfer in small pores of the membrane is affected by the collision of transferred modules and membrane wall. This effect can be defined by the Knudsen equation as follows [38]:

$$D_{knd}=\frac{2}{3}d_p\sqrt{\frac{2RT}{\pi M_v}} \tag{7}$$

where d_p is pore diameter (m) and R represents universal gas constant (Pa $m^3\ mol^{-1}\ K^{-1}$). Furthermore, T and M_V indicate temperature (K) and vapor molecular weight (kg mol^{-1}), respectively. The Knudsen number was calculated and its average value was 11.6. To finalize the diffusion coefficient definition, membrane structure properties must be considered as following equations [32]:

$$D_{AB,eff}=\frac{\varepsilon D_{AB}}{\tau} \tag{8}$$

$$D_{knd,eff}=\frac{\varepsilon D_{knd}}{\tau} \tag{9}$$

in which $D_{AB,eff}$ is modified gases diffusion coefficient ($m^2\ s^{-1}$), $D_{knd,eff}$ is modified Knudsen diffusion coefficient ($m^2\ s^{-1}$), ε is porosity and τ is tortuosity of the membrane. The effective diffusion coefficient (D_{eff}) was obtained using the Bonsaquet equation as follows [39]:

$$\frac{1}{D_{eff}}=\frac{1}{D_{AB,eff}}+\frac{1}{D_{knd,eff}} \tag{10}$$

To calculate mass transfer in the membrane, it should be considered that only diffusion contributes in mass transfer. Therefore, Eq. (11) was used as a simplified mass transfer equation to qualify diffusive flux in the membrane [36].

$$\nabla\cdot\left(D_{eff}\nabla C_v\right)=0 \tag{11}$$

where C_v indicates the vapor molar concentration in the membrane (mol m^{-3}).

2.1.3. Thermodynamic

To calculate interfacial vapor pressure, the solution was considered to be ideal based on Raoul's law. According to this assumption, the vapor pressure is calculated using Eqs. (12) and (13) [40].

$$P_{water}=x_w P_{sat-water} \tag{12}$$

$$P_{EG}=x_{EG}P_{sat-EG} \tag{13}$$

in which X_w, X_{EG}, $P_{sat\text{-}water}$, $P_{sat\text{-}EG}$ present water mole fraction, *EG* mole fraction, water saturation pressure (Pa) and *EG* saturation pressure (Pa), respectively.

Antoine's law was used here to relate pure water saturation pressure to temperature [14]:

$$P_{sat,pure\ water}=1000e^{\left(16.3872-\frac{3885.2}{T-42.96}\right)} \tag{14}$$

Ethylene Glycol saturation pressure was calculated using Eq. (15) [41].

$$P_{sat\ EG}=\left(\frac{100000}{760}\right)*\left(10^{8.21211-\frac{2161.91}{\mathrm{T}-273.15+208.43}}\right) \tag{15}$$

where T is the temperature in the interface (K), which was determined using Eq. (23). Dissolving EG in water affects the water purity, Eq. (16) is to obtain water mole fraction in solution.

$$x_w=1-x_{EG} \tag{16}$$

where X_{EG} and X_W are mole fraction of *EG* and water in solution, respectively. By solving the mass transfer equation, each species concentration will be obtained. In order to perform solution thermodynamic studies, Eq. (17) is derived based on mass balance law which relates the EG concentration to the EG mole fraction [36].

$$x_{EG}=\frac{C_{EG}M_{EG}/\rho_{EG}}{1-(M_{EG}/\rho_{EG}-M_w/\rho_w)C_{EG}} \tag{17}$$

in which C_{EG}, M_{EG}, ρ_{EG}, M_W and ρ_W are EG molar concentration (mol m^{-3}), *EG* molecular weight (kg mol^{-1}), *EG* density

(kg m^{-3}), water molecular weight (kg mol^{-1}) and water density (kg m^{-3}), respectively.

The base of VMD is evaporating the liquid phase at the intersection of membrane and feed. The vapor generated at the intersection is the main parameter of mass transfer driving force production through the membrane side. To ensure the accuracy of the results, the calculated vapor pressure by Raoul's law were compared with the predicted values by the HYSYS software as presented in Table 2. The vapor pressure of water was calculated using Eq. (18) [40].

$$x_w y_w P_w^{sat} = y_w P \tag{18}$$

And similarly for *EG*, Eq. (19) was used to calculate its vapor pressure [40].

$$x_{EG} y_{EG} P_{EG}^{sat} = y_{EG} P \tag{19}$$

According to the Raoult's law that assumes the solution to be ideal and activity coefficient equal to 1, Eq. (20) was simply used [40].

$$P = x_w P_w^{sat} + x_{EG} P_{EG}^{sat} \tag{20}$$

One of the most serious matters in thermodynamic science is activity coefficients calculation and a modern method to calculate these factors is UNIQUAC. However, this equation is complex and it is hard to input the UNIQUAC equation to the COMSOL Multiphysics Software. Therefore, the calculated vapor pressure using the UNIQUAC method was used as a reference vapor pressure. In the first phase of the thermodynamic simulation, the calculated vapor pressure using the UNIQUAC method was compared with the calculated vapor pressure using the Raoult's law as outlined in Table 2.

Based on the results indicated in Table 2, the Raoult's law error with respect to the UNIQUAC model is on average 1.6054% and acceptable. In the second phase of the thermodynamic simulation, the Margules activity law as one of the most fundamental models was used. Although this model is rarely used today in industrial simulations, in terms of simplicity for using in the COMSOL Multiphysics software is suitable. The Margules model for the two components solution of water and EG is shown using Eqs. (21) and (22) [40].

$$\ln\left(\gamma_w\right) = A x_{EG}^2 \tag{21}$$

$$\ln\left(\gamma_{EG}\right) = A x_w^2 \tag{22}$$

where A is a constant that is related to molecular size, γ_w is water activity coefficient and γ_{EG} is EG activity coefficient. The unknown amount of A should be calculated via a linear method. In this study, the linear method was performed by a goal seek function in the Excel software with fitting. The numerical value of A was obtained –0.01741 and as a result, the error reduced from 1.6054 to 1.3619. The results are presented in Table 2.

2.1.4. Overall heat transfer

Transmembrane mass transfer in VMD is directly related to thermal conditions in the process, therefore it is crucial to perform an accurate temperature calculation. A simplification of the general energy balance equation was

Table 3
Boundary conditions in the feed side

	Position	Type	Equation
Momentum transfer	$x = 0$	Inlet velocity	$U = U_0$
	$x = L$	Pressure	P = 1 atm
	$y = y_2$	Wall	U = 0
	$y = y_3$	Wall	U = 0
Heat transfer	$x = 0$	Constant temperature	$T = T_0$
	$x = L$	Outflow	$K\nabla T = 0$
	$y = y_2$	Boundary heat source	$Q = (\partial C_v/(\partial y)\, D_{eff} M_w L_w$
	$y = y_3$	Symmetry	$\partial T/\partial y = 0$

Table 2
Calculated and predicted water vapor pressure

EG mass fraction (%)	EG mole fraction (%)	T (°C)	Saturation pressure (kPa)			Error (%)	
			UNIQUAC	Rault's law	Margules	Raults law	Margules
0.2	0.0676	40	6.850733	6.8354	6.732743	0.2238	1.7222
0.2	0.0676	50	11.46891	11.426	11.2544	0.3741	1.8703
0.2	0.0676	60	18.53508	18.572	18.29308	0.1992	1.3056
0.4	0.1621	40	6.066929	6.147	6.072338	1.3197	0.0891
0.4	0.1621	50	10.18496	10.31	10.18477	1.2276	0.0018
0.4	0.1621	60	16.50316	16.709	16.50605	1.2473	0.0175
0.6	0.3033	40	4.932943	5.1183	5.075239	3.7575	2.8846
0.6	0.3033	50	8.318878	8.588	8.515748	3.2350	2.3665
0.6	0.3033	60	13.53717	13.925	13.80785	2.8649	1.9995
					Average	1.6054	1.3619

Table 4
Boundary conditions in the permeate side

	Position	Type	Equation
Momentum transfer	$x = 0$	No slip condition	U = 0
	$x = L$	Pressure	P = 0
	$y = y_0$	No-slip condition	U = 0
	$y = y_1$	Inlet velocity	$U = \frac{\left(\frac{\partial C_{mem.}/\partial y}{vapor}\right) D_{eff} M_w}{\rho_v}$
Heat transfer	$x = 0$	Insulation	$\partial T/\partial x = 0$
	$x = L$	Convective outflow	$K\nabla T = 0$
	$y = y_0$	Symmetry	$\partial T/\partial y = 0$
	$y = y_1$	Temperature	$T = T_{mem.}$

Table 5
Boundary conditions in the membrane

	Position	Type	Equation
Mass transfer	$x = 0, x = L$	Insulation	$J_v = 0$
	$y = y_1$	Concentration	Pvac/RT
	$y = y_2$	Concentration	Psat/RT
Heat transfer	$x = 0, x = L$	Insulation	$\partial T/\partial x = 0$
	$y = y_1$	Temperature	$T = T_{Permeate.}$
	$y = y_2$	Boundary heat source	$(\partial C/(\partial y)\, D_{eff} M_w L_w$

leaded to obtain Eq. (23) and it is used to obtain temperature in the feed and the permeate sides [42]:

$$\rho_w C_{p,w} u \cdot \nabla T = \nabla \cdot \left(k_w \cdot \nabla T\right) \tag{23}$$

in which ρ_w, C_p and k are density (kg m^{-3}), specific heat capacity (J mol^{-1} K^{-1}), and thermal conductivity (W m^{-1} K^{-1}), respectively. Velocity vector in Eq. (23) was obtained via Eq. (2). Therefore the overall heat transfer in the membrane is as follows [42]:

$$\rho_m C_{p,m} u \cdot \nabla T = \nabla \cdot \left(k_m \cdot \nabla T\right) \tag{24}$$

in this equation, ρ_m and CP_m are density (Kg m^{-3}) and specific heat capacity (J mol^{-1} K^{-1}) of the membrane. Furthermore, K_m is the membrane thermal conductivity (W m^{-1} K^{-1}) that is the average thermal conductivity of the membrane polymer material and the flowing vapour as calculated using Eq. (25) [32].

$$K_m = \varepsilon K_v + (1-\varepsilon) K_{pol.} \tag{25}$$

where K_v is water vapor thermal conductivity (W m^{-1} K^{-1}) and K_p is polymer thermal conductivity (W m^{-1} K^{-1}). Heat consumption is occurred in the membrane-feed interface due to water evaporation. Combining conservation laws of heat and mass was caused to providing Eq. (26). It was implemented to compute total heat consumed by evaporation per unit area of the membrane [42].

$$Boundary\ heat\ flux = (\partial C_v / \partial y) D_{eff} M_w L_w \tag{26}$$

in which M_w and L_w are water molecular weight (kg k mol^{-1}) and enthalpy of vaporization (KJ kg^{-1}), respectively. Since the permeate side is always considered to be pure, there was no mass transfer condition in this system. Thus, there was no need to solve mass transfer for this subdomain and just momentum and heat transfer were solved (Table 4).

Temperature polarization coefficient is defined as the ratio of local membrane-feed interfacial temperature to feed temperature as Eq. (27) [43]:

$$TPC = \frac{T_{mem-feed}}{T_{feed}} \tag{27}$$

where $T_{mem\text{-}feed}$ and T_{feed} are local membrane-feed interfacial temperature and feed temperature, respectively.

2.2. Numerical algorithm

In this research, the model equations and the involving nonlinear PDEs with related boundary conditions were solved using the COMSOL Multiphysics software (version 4.3b). Heat, momentum and mass transfer were evaluated simultaneously with consideration of their interaction with each other. The algorithms of coupling were solved in COMSOL Multiphysics. Furthermore, a numerical solution algorithm involves discretization which was carried out using FEM. In Fact, mesh generation is a key point in a numerical simulation for getting accurate results that should be optimized (elements types and number). For this purpose, initial guess should be determined carefully because of the non-linear nature of PDEs. Moreover, a non-wetted approach also was assumed for numerical simulation of the flat module.

2.3. Validation

The simulation validation was performed using the comparison of feed temperature, EG concentration and feed flow rate effects on permeate flux with the experimental data reported by Akbarabadi et al. [2].

3. Results and discussion

3.1. Mesh optimization

In order to find optimum mesh, proper elements types and optimum elements number should be determined. Thus, proper elements types were determined using software offer as "extra fine mesh" in its mesh setting section. The proper elements types were included triangular, quadrilateral, edge and vertex elements. It should be mentioned that triangular elements are proper for subdomain interior. Furthermore, it is better to use a different type of mesh for walls and angles subdomains for instance on walls it is better to use structured elements (4 pointed) like quadrilateral element due to the high gradient in these areas. This mesh is automatically created and adapted for the model's physics settings. The resulting mesh is able to solve the geometry quite well, it does so in all regions of the geometry even

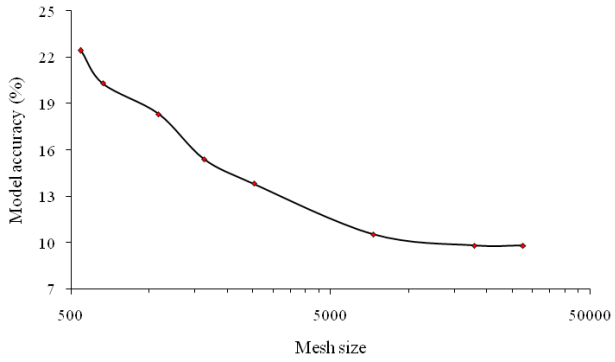

Fig. 2. Effect of mesh size on model accuracy.

where much fewer elements would be adequate to use for meshing, thus reducing memory requirements. In fact, the meshing algorithms in COMSOL Multiphysics try to avoid low-quality elements, however it is not always possible to do so for all geometries. Depending on the quality measure used the Average element quality changes accordingly. To get accurate results, it is important to know which Average element quality is sufficient for any particular application. An optimum elements number was determined in the range of 545 to 27557 elements. As shown in Fig. 2, it was found that increasing mesh number more than 17864 elements doesn't affect accuracy significantly. Overall, the optimum elements number was 17864 which 16814 elements were triangular, 1050 elements were quadrilateral, 739 elements were edge and 8 elements were vertex. For this simulation, average mesh quality is 0.9119 which indicates an optimal element in the chosen quality measure.

3.2. Effect of operating parameters

3.2.1. Feed temperature

Effect of feed temperature on permeate is indicated in Fig. 3. The most important and effective parameter in VMD process is temperature due to its significant role in permeate flux. It was observed that permeate flux increases with increasing feed temperature [15,44,45]. The partial pressure of water vapor increases in the feed-membrane interface as a result of temperature increment. In fact, since the main driving force of VMD is the partial pressure gradient of water vapor through the membrane, increasing feed temperature leads to permeate flux enhancement [33,46].

3.2.2. Feed concentration

Effect of feed concentration on permeate flux is shown in Fig. 4. As observed, permeate flux decreases with increasing EG concentration. It is due to ethylene glycol boiling point (197.6°C) which is relatively high in comparison to that of water and results in its very low vapor pressure. Therefore, the EG addition leads to the decreasing water activity coefficient in the feed side and thus permeate flux slightly reduces. Since the partial pressure gradient of water vapor through the membrane is the basic driving force of VMD process, reduction of permeate flux with further increasing of feed concentration can be due to the reduction of driving force [45].

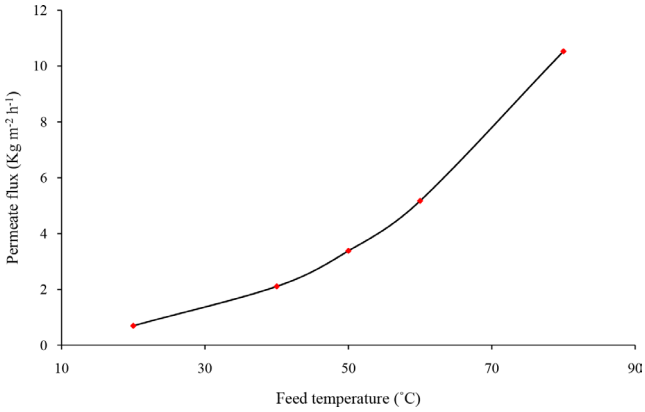

Fig. 3. Effect of feed temperature on permeate flux (Q_{0F} = 0.8 Lmin^{-1}, C_{EG} = 60 wt. %).

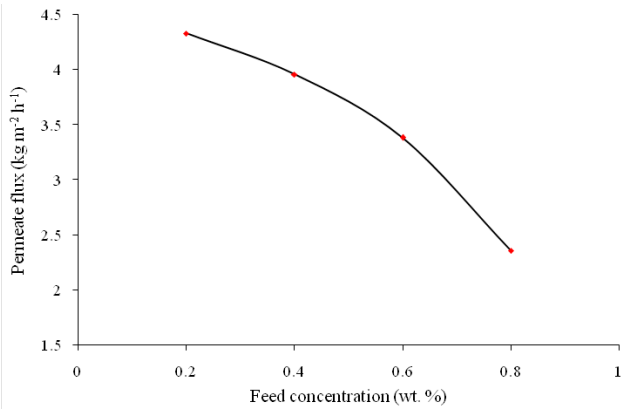

Fig. 4. Effect of feed concentration on permeate flux (T_{0F} = 50°C, Q_{0F} = 0.8 L min^{-1}).

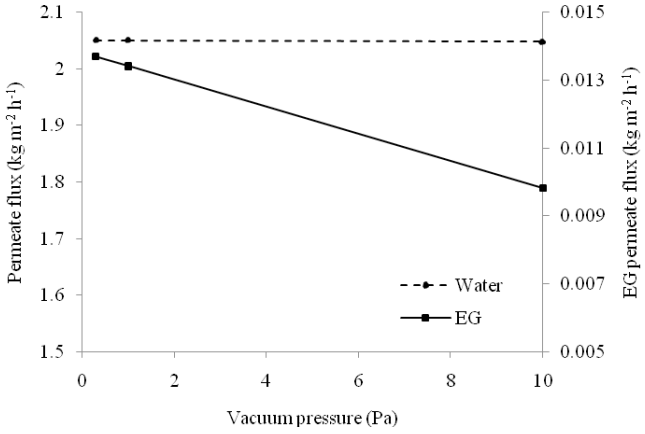

Fig. 5. Effect of vacuum pressure on permeate flux (T_{0F} = 40°C, Q_{0F} = 0.4 L min^{-1}, C_{EG} = 60 wt. %).

3.2.3. Vacuum pressure

Effect of feed vacuum pressure in the permeate side on permeate flux is illustrated in Fig. 5. It can be seen that in the region with lower vacuum pressure, by increasing evaporation rate, vapor velocity in the membrane vicinity

of the permeate side increases. Furthermore, concentration polarization in the feed-membrane interface increases [32]. Therefore, permeate vacuum pressure decrement by the driving force increment leads to increasing permeate flux and decreasing EG selectivity [47].

3.3. Effect of membrane characteristics

3.3.1. Porosity

Membrane porosity is the ratio of the pores volume over the total volume of the membrane as defined by Franken and Rippergerin 1988 and Smolders and Franken in 1989 [48]. Generally, membrane porosity is an important parameter affecting VMD permeate flux due to larger evaporation surface area of the more porous membrane. In fact, membranes with higher porosity exhibit higher permeate flux and lower conductive heat flux [15,33]. Effect of membrane porosity on permeate flux is illustrated in Fig. 6. Porosity has direct effects on diffusion coefficients as observed in Eqs. (8) and (9), thus with increasing membrane porosity, permeate flux increases [33].

3.3.2. Pore size

One of the important parameters in order to achieve high efficiency in VMD is the membrane pore size. It's ascribed to the fact that membrane pore size increment results in mass transfer resistance decrement and consequently permeate flux increment [33]. In addition, pore size distribution should be as narrow as possible due to preventing liquid feed penetration into the pores. Therefore, it is crucial to determine optimum pore size and pore size distribution for each operating condition and feed solution in order to achieve high productivity [48]. Effect of membrane pore size on permeate flux is indicated in Fig. 6. Pore size has a direct effect on the diffusion coefficient based on Eq. (7). As shown in Fig. 7, permeate flux slightly increases with increasing membrane pore size. [15].

3.3.3. Thickness

Membrane thickness is another considerable characteristic in VMD processes. This is due to the fact that the thicker membrane has the longer path and the bigger resistance along membrane module, thus the thinner membrane is needed to obtain higher permeate flux [33]. Effect of membrane thickness on permeate flux is shown in Fig. 8. As can be observed, increasing membrane thickness reduces permeate flux due to the mass transfer resistance increment. At the same time, it results in heat loss reduction [33]. Generally, there is an inverse relationship between the permeate flux and membrane thickness [15,32].

3.4. Field distribution

3.4.1. Velocity

Permeate side velocity distribution along the module is presented in Fig. 9. As observed in this simulation, the velocity at the membrane wall is nearly negligible but not zero which is the same as real situations. It is because of the fact that membrane-permeate interface has more area than outflow. The vapor permeated from membrane wall is accumulated in outflow, making a higher flow velocity in that interface. It is also larger at the center in comparison to boundary. Moreover, all the permeate gathers together, thus permeate flow reaches to its maximum value in the outlet and exits from the module [49]. It is notable that permeate side velocity distribution of membrane contractor was simulated by solving Navier–Stokes equations [27,50].

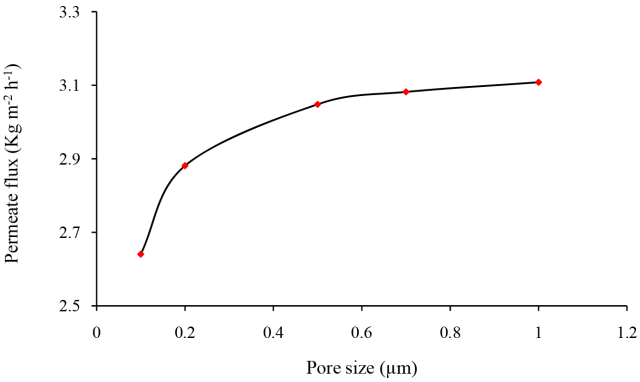

Fig. 7. Effect of membrane pore size on permeate flux (T_{0F} = 40°C, Q_{0F} = 0.4 L min^{-1}, C_{EG} = 20 wt. %).

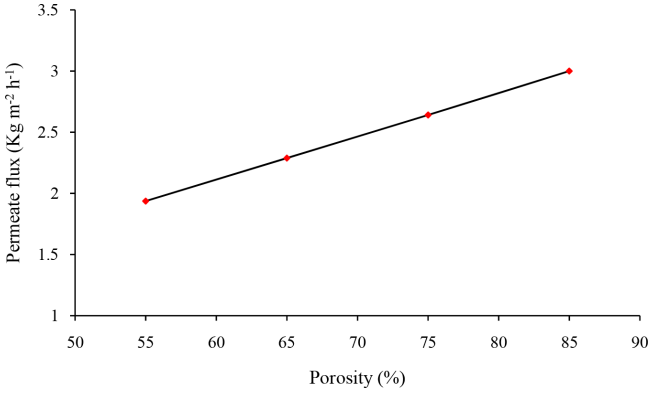

Fig. 6. Effect of membrane porosity on permeate flux (T_{0F} = 40°C, Q_{0F} = 0.4 L min^{-1}, C_{EG} = 20 wt. %).

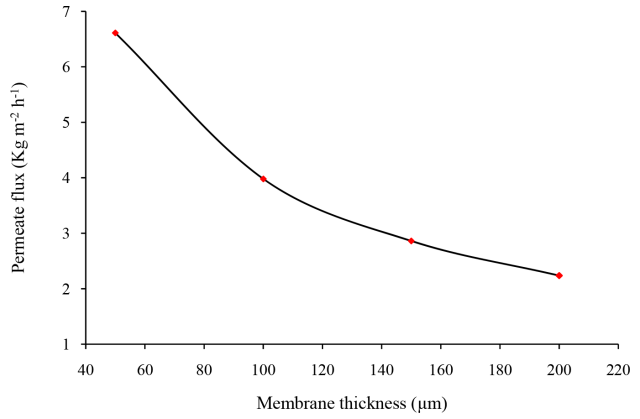

Fig. 8. Effect of membrane thickness on permeate flux (T_{0F} = 40°C, Q_{0F} = 0.4 L min^{-1}, C_{EG} = 20 wt. %).

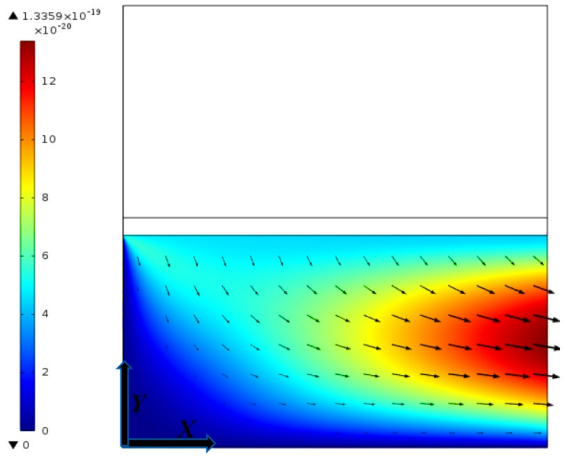

Fig. 9. Permeate side velocity distribution along the module (T_{0F} = 40°C, C_{EG} = 60 wt. %).

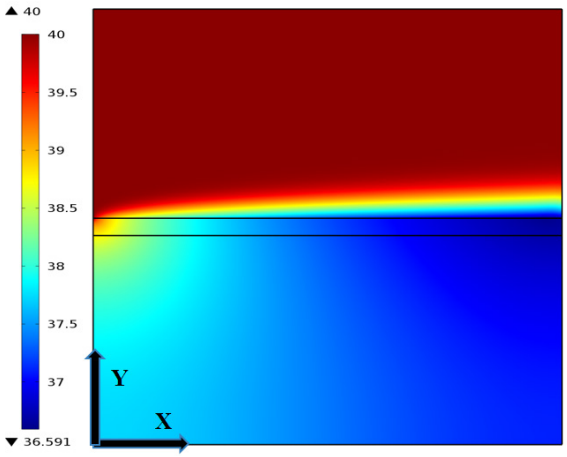

Fig. 10. Temperature distribution along the module (T_{0F} = 40°C, Q_{0F} = 0.4 L min^{-1}, C_{EG} = 60 wt. %).

3.4.2. Temperature

Temperature distribution along the module is indicated in Fig. 10. As it can be seen, feed evaporation in the feed-membrane interface causes the feed temperature reduction along its route, while the permeate vapor temperature rises as it leaves the module. On the other hand, when the permeate vapor leaves the membrane, it receives more heat. These are because of its non-direct counter-current contact with feed [32,44]. Fig. 10 shows that the temperature in the majority of the feedside is uniform but there is a thin temperature gradient region near feed-membrane interface which causes unwanted temperature polarization [51]. Temperature polarization coefficient (TPC) is defined as the ratio of the local membrane-feed interfacial temperature to the feed temperature [43]. TPC along the membrane-feed interface as dimensionless module length is shown in Fig. 11. As presented, TPC is at its highest value in the module inlet which indicates better heat transfer in the feed side of the module. However, it decreases along the feed path due to temperature reduction resulted from evaporation.

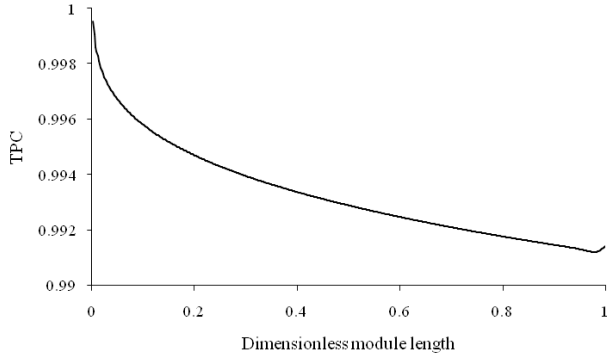

Fig. 11. TPC along the membrane-feed interface (T_{0F} = 40°C, Q_{0F} = 0.8 L min^{-1}, C_{EG} = 60 wt. %).

3.4.3. Concentration

Given that actual feeds have different concentration; feed concentration investigation is a useful tool to determine the VMD process performance. Therefore, solute concentration should be calculated precisely to achieve better concentration distribution understanding and study concentration gradient effects [52]. Concentration distribution along the membrane is illustrated in Fig. 12. As observed, a very thin concentration gradient layer is formed in the membrane vicinity of the feed side which causes an intensive concentration increment on the membrane surface. This makes an undesired effect on vapor pressure in the membrane-feed interface. Water evaporation causes temperature depletion along the module which results in mass transfer driving force reduction. It also illustrated that the vapor concentration gradient at the module inlet side (left side) is larger compared with the module outlet side (right side) [32].

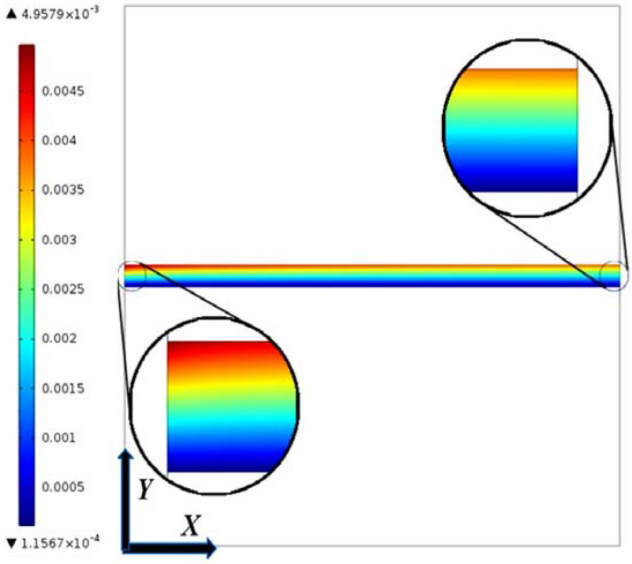

Fig. 12. Concentration distribution along the membrane (T_{0F} = 40°C, Q_{0F} = 0.4 L min^{-1}, C_{EG} = 60 wt. %).

3.5. Flux along the module

In this research, a mass transfer mechanism was presented in order to obtain permeate flux resulted from chemical potential gradient [30]. Permeate flux as a function of dimensionless module length is shown in Fig. 13. It can be observed that permeate flux decreases along the flow path. The main reason is the temperature decrement as driving force resulted from evaporation [32,33,45].

3.6. Validation

Comparison of feed temperature effect on permeate flux for simulated and experimental results are presented in Fig. 14, where feed temperature was varied from 40 to 60°C. Furthermore, comparison of feed flow rate effect on permeate flux for simulated and experimental results are shown in Fig. 15. For this purpose, the feed flow rate was considered in the range of 0.3–0.8 L min^{-1}. Moreover, comparison of feed concentration effect on the permeate flux for simulated and experimental results are displayed in Fig. 16. The feed concentration was investigated from 20 to 60 wt.%. It can be seen that in all of the comparisons simulated and experimental results are in good agreement. This confirms that the two-dimensional model extended in this research for VMD process can predict performance accurately.

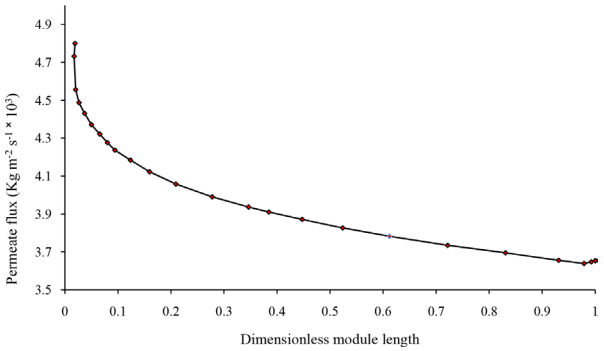

Fig. 13. Flux distribution along the module (T_{0F} = 40°C, Q_{0F} = 0.4 L min^{-1}, C_{EG} = 60 wt. %).

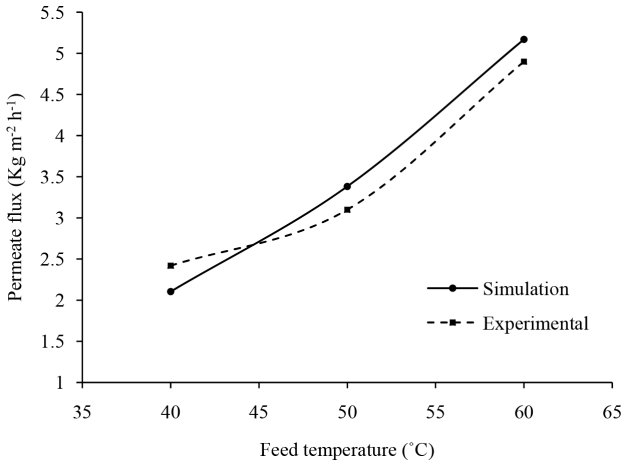

Fig. 14. Comparison of feed temperature effect on permeate flux for simulated and experimental results (Q_{0F} = 0.8 L min^{-1}, C_{EG} = 60 wt. %).

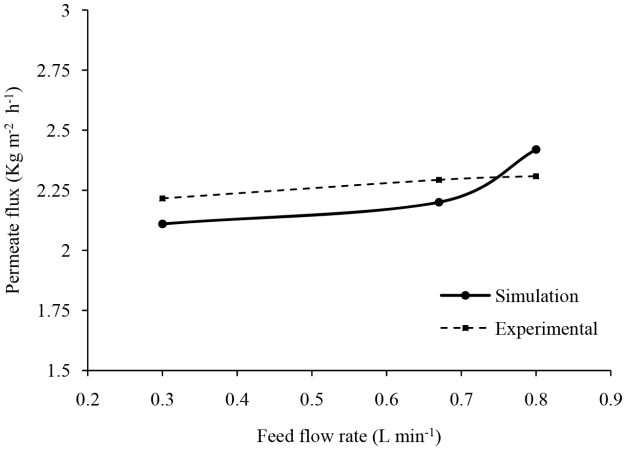

Fig. 15. Comparison of feed flow rate effect on permeate flux for simulated and experimental results (T_{0F} = 40°C, C_{EG} = 60 wt. %).

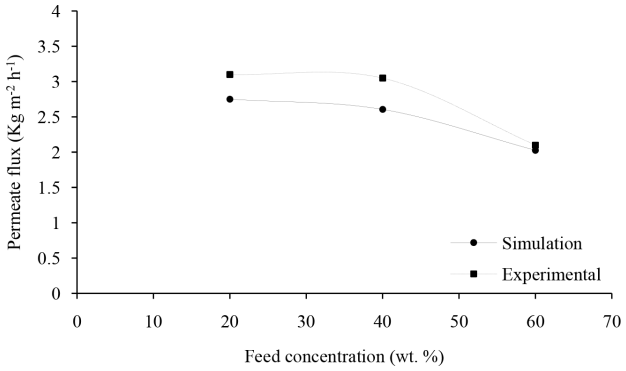

Fig. 16. Comparison of feed concentration effect on permeate flux for simulated and experimental results (T_{0F} = 40°C, Q_{0F} = 0.3 L min^{-1}).

4. Conclusion

Vacuum membrane distillation simulation of water extraction from EG solution as a volatile material using a flat PP membrane was studied in this research. Computational fluid dynamics was the method used to solve PDEs numerically. Finite element method which is a common discretization method in CFD was found to be a convenient method to solve coupled heat, mass and Navier-Stokes PDEs. Furthermore, the fugacity coefficient was used in order to calculate vapor and liquid activity coefficients. To ensure the accuracy of the results, the calculated vapor pressure values by the Raoul's law were compared with the predicted values by the HYSYS software. Moreover, it was investigated by numerical methods. Effects of operating parameters comprising feed temperature, feed concentration and vacuum pressure and effects of membrane characteristics including porosity, pore size and thickness on permeate flux were studied. Furthermore, field distributions (velocity, temperature and concentration) and permeate flux along the module

were investigated. The results also showed that the temperature is the most affecting parameter since vapor pressure is exponentially dependent on temperature. Reduction of downstream permeate pressure resulted in increasing the driving force which is a vapor pressure gradient between the two sides of the membrane pores. Consequently, this leads to permeate flux enhancement. There is an inversely proportional relationship between feed concentration and permeate flux. In other words, the addition of EG reduces water activity coefficient in the feed and hence pure water flux slightly decreases. Furthermore, it was found out that membranes with higher porosity have larger evaporation surface area, higher permeate flux and lower conductive heat flux. Moreover, membrane pore size increment causes mass transfer resistance decrement in the membrane pores, and thus permeate flux increment. Additionally, membrane thickness is another considerable characteristic in VMD processes. The thicker membrane provides more resistance along the module so in order to obtain higher VMD permeate flux, the membrane should be as thin as possible. This model has shown to be reusable for studying VMD involving various aqueous solutions.

Acknowledgment

The authors would like to thank Iran National Science Foundation (INSF) for supporting the research (Grant No. 96008182).

Symbols

C — Concentration (mol m^{-3})
C_p — Specific heat capacity (J mol^{-1} K^{-1})
C_v — Molar concentration of vapor (mol m^{-3})
D_{AB} — Gases diffusion coefficient (m^2 s^{-1})
$D_{AB,eff}$ — Modified gases diffusion coefficient (m^2 s^{-1})
D_{eff} — Effective diffusion coefficient (m^2 s^{-1})
D_{knd} — Knudsen diffusion coefficient (m^2 s^{-1})
$D_{knd,eff}$ — Modified Knudsen diffusion coefficient (m^2 s^{-1})
d_p — Pore diameter (m)
ε — Porosity (%)
ε'_{AB} — Energy of molecular attraction (J)
$f(kT\,\varepsilon_{AB}^{-1})$ — Collision function
k' — Boltzmann constant (J K^{-1})
K_m — Membrane thermal conductivity (W m^{-1} K^{-1})
K_p — Polymer thermal conductivity (W m^{-1} K^{-1})
K_v — Vapor thermal conductivity (W m^{-1} K^{-1})
L_w — Enthalpy of vaporization (KJ kg^{-1})
M_{EG} — EG molecular weight (kg mol^{-1})
M_w — Water molecular weight (kg mol^{-1})
P — Pressure (Pa)
$P_{sat\text{-}EG}$ — EG saturated pressure (Pa)
$P_{sat\text{-}water}$ — Water saturated pressure (Pa)
P_t — Absolute pressure (Pa)
r — Collision diameter (nm)
R — Universal gases constant (Pa m^3 mol^{-1} K^{-1})
T — Temperature (K)
T_b — Boiling point (K)
u — Velocity (m s^{-1})
x_{EG} — EG mole fraction in the liquid phase
x_w — Water mole fraction in the liquid phase
y_{EG} — EG mole fraction in the vapor phase
y_w — Water mole fraction in the vapor phase
γ_{EG} — EG activity coefficient
γ_w — Water activity coefficient
μ — Dynamic viscosity (Pa·s)
ρ — Density (kg m^{-3})
τ — Tortuosity
υ — Molecular volume (m^3 mol^{-1})

References

[1] K. Jardak, A. Dirany, P. Drogui, M.A. El Khakani, Statistical optimization of electrochemical oxidation of ethylene glycol using response surface methodology, Process Saf. Environ. Prot., 105 (2017) 12–20.
[2] T. Mohammadi, M. Akbarabadi, Separation of ethylene glycol solution by vacuum membrane distillation (VMD), Desalination, 181 (2005) 35–41.
[3] V.K. Gupta, I. Ali, T.A. Saleh, A. Nayak, S. Agarwal, Chemical treatment technologies for waste-water recycling—an overview, Rsc Adv., 2 (2012) 6380–6388.
[4] D. Allende, D. Pando, M. Matos, C.E. Carleos, C. Pazos, J.M. Benito, Optimization of a membrane hybrid process for oil-in-water emulsions treatment using Taguchi experimental design, Desal. Water Treat., 57 (2016) 4832–4841.
[5] B. Van der Bruggen, C. Vandecasteele, T. Van Gestel, W. Doyen, R. Leysen, A review of pressure-driven membrane processes in wastewater treatment and drinking water production, Environ. Prog., 22 (2003) 46–56.
[6] H. Strathmann, Membrane separation processes, J. Membr. Sci., 9 (1981) 121–189.
[7] Z.-B. Chen, Z.-Q. Chen, N.-Q. Ren, H.-C. Wang, S.-K. Nie, M.-H. Cui, Modeling of mixed liquor inorganic suspended solids and membrane flux at different ratio of SRT to HRT in a submerged membrane bioreactor, Appl. Math. Modell., 36 (2012) 173–182.
[8] J.R. Scheibler, E.R.F. Santos, A.S. Barbosa, M.G.F. Rodrigues, Performance of zeolite membrane (ZSM-5/γ-Alumina) in the oil/water separation process, Desal. Water Treat., 56 (2015) 3561–3567.
[9] Q. Chang, X. Wang, Y. Wang, X. Zhang, S. Cerneaux, J.-e. Zhou, Effect of hydrophilic modification with nano-titania and operation modes on the oil–water separation performance of microfiltration membrane, Desal. Water Treat., 57 (2016) 4788–4795.
[10] K. Majewska-Nowak, J. Kawiecka-Skowron, Ceramic membrane behaviour in anionic dye removal by ultrafiltration, Desal. Water Treat., 34 (2011) 367–373.
[11] S.K. Nataraj, K.M. Hosamani, T.M. Aminabhavi, Distillery wastewater treatment by the membrane-based nanofiltration and reverse osmosis processes, Water Res., 40 (2006) 2349–2356.
[12] M. Godino, L. Peña, C. Rincón, J. Mengual, Water production from brines by membrane distillation, Desalination, 108 (1997) 91–97.
[13] E. Curcio, E. Drioli, Membrane distillation and related operations—a review, Sep. Purif. Rev., 34 (2005) 35–86.
[14] K.W. Lawson, D.R. Lloyd, Membrane distillation, J. Membr. Sci., 124 (1997) 1–25.
[15] A. Alkhudhiri, N. Darwish, N. Hilal, Membrane distillation: A comprehensive review, Desalination, 287 (2012) 2–18.
[16] Z. Ding, L. Liu, Z. Liu, R. Ma, The use of intermittent gas bubbling to control membrane fouling in concentrating TCM extract by membrane distillation, J. Membr. Sci., 372 (2011) 172–181.
[17] M. El-Bourawi, Z. Ding, R. Ma, M. Khayet, A framework for better understanding membrane distillation separation process, J. Membr. Sci., 285 (2006) 4–29.
[18] J. Zhang, S. Gray, Modelling heat and mass transfers in DCMD using compressible membranes, J. Membr. Sci., 387 (2012) 7–16.
[19] M. Khayet, Membrane distillation, Adv. Membr. Technol. Applic., (2008) 297–369.

[20] S. Al-Asheh, F. Banat, M. Qtaishat, M. Al-Khateeb, Concentration of sucrose solutions via vacuum membrane distillation, Desalination, 195 (2006) 60–68.
[21] S. Bandini, A. Saavedra, G.C. Sarti, Vacuum membrane distillation: experiments and modeling, AIChE J., 43 (1997) 398–408.
[22] J. Liu, Q. Wang, L. Han, B. Li, Simulation of heat and mass transfer with cross-flow hollow fiber vacuum membrane distillation: The influence of fiber arrangement, Chem. Eng. Res. Des., 119 (2017) 12–22.
[23] R. Bagger-Jørgensen, A.S. Meyer, C. Varming, G. Jonsson, Recovery of volatile aroma compounds from black currant juice by vacuum membrane distillation, J. Food Eng., 64 (2004) 23–31.
[24] J. Zuo, T.-S. Chung, G.S. O'Brien, W. Kosar, Hydrophobic/hydrophilic PVDF/Ultem® dual-layer hollow fiber membranes with enhanced mechanical properties for vacuum membrane distillation, J. Membr. Sci., 523 (2017) 103–110.
[25] F. Banat, S. Al-Asheh, M. Qtaishat, Treatment of waters colored with methylene blue dye by vacuum membrane distillation, Desalination, 174 (2005) 87–96.
[26] S. Upadhyaya, K. Singh, S. Chaurasia, R.K. Dohare, M. Agarwal, Mathematical and CFD modeling of vacuum membrane distillation for desalination, Desal. Water Treat., 57 (2016) 11956–11971.
[27] N. Tang, H. Zhang, W. Wang, Computational fluid dynamics numerical simulation of vacuum membrane distillation for aqueous NaCl solution, Desalination, 274 (2011) 120–129.
[28] X. Wei, H. Wang, Z. Yin, S. Qaseem, J. Li, Tubular electrocatalytic membrane reactor for alcohol oxidation: CFD simulation and experiment, Chin. J. Chem. Eng., 25 (2017) 18–25.
[29] S. Wardeh, H.P. Morvan, CFD simulations of flow and concentration polarization in spacer-filled channels for application to water desalination, Chem. Eng. Res. Des., 86 (2008) 1107–1116.
[30] V. Soni, J. Abildskov, G. Jonsson, R. Gani, Modeling and analysis of vacuum membrane distillation for the recovery of volatile aroma compounds from black currant juice, J. Membr. Sci., 320 (2008) 442–455.
[31] N. Diban, O.C. Voinea, A. Urtiaga, I. Ortiz, Vacuum membrane distillation of the main pear aroma compound: Experimental study and mass transfer modeling, J. Membr. Sci., 326 (2009) 64–75.
[32] H. Hayer, O. Bakhtiari, T. Mohammadi, Analysis of heat and mass transfer in vacuum membrane distillation for water desalination using computational fluid dynamics (CFD), Desal. Water Treat., 55 (2015) 39–52.
[33] S.G. Lovineh, M. Asghari, B. Rajaei, Numerical simulation and theoretical study on simultaneous effects of operating parameters in vacuum membrane distillation, Desalination, 314 (2013) 59–66.
[34] S. Heile, S. Rosenberger, A. Parker, B. Jefferson, E. McAdam, Establishing the suitability of symmetric ultra thin wall polydimethylsiloxane hollow-fibre membrane contactors for enhanced CO_2 separation during biogas upgrading, J. Membr. Sci., 452 (2014) 37–45.
[35] V.L. Streeter, E.B. Wylie, K.W. Bedford, Fluid mechanics. WCB, McGraw-Hill, 1998.
[36] R.E. Treybal, Mass Transfer Operations, New York, 1980.
[37] M. Khayet, Membranes and theoretical modeling of membrane distillation: a review, Adv. Colloid Interface Sci., 164 (2011) 56–88.
[38] F. Chen, R. Mourhatch, T.T. Tsotsis, M. Sahimi, Pore network model of transport and separation of binary gas mixtures in nanoporous membranes, J. Membr. Sci., 315 (2008) 48–57.
[39] R.H. Perry, D.W. Green, Perry's chemical engineers' handbook, McGraw-Hill Professional 1999.
[40] J. Smith, H. Van Ness, M. Abbott, Chemical engineering thermodynamics, Sat, 18 (1996) 1–3.
[41] W. Jones, W. Tamplin, Physical properties of propylene glycol, Reinhold: New York 1952.
[42] J. Holman, Heat transfer, 1986, Mc Gran–Hill Book Company, Soythern Methodist University, (1986).
[43] Y. Yang, D. Rana, T. Matsuura, C.Q. Lan, The heat and mass transfer of vacuum membrane distillation: effect of active layer morphology with and without support material, Sep. Purif . Technol., 164 (2016) 56–62.
[44] J. Zhang, M. Duke, M. Hoang, Z. Xie, A. Groth, C. Tun, S. Gray, Modelling of vacuum membrane distillation, J. Membr. Sci., 434 (2013) 1–9.
[45] T. Mohammadi, P. Kazemi, Taguchi optimization approach for phenolic wastewater treatment by vacuum membrane distillation, Desal. Water Treat., 52 (2014) 1341–1349.
[46] F. Jia, J. Li, J. Wang, Y. Sun, Removal of strontium ions from simulated radioactive wastewater by vacuum membrane distillation, Ann. Nucl. Energy, 103 (2017) 363–368.
[47] F.A. Banat, J. Simandl, Removal of benzene traces from contaminated water by vacuum membrane distillation, Chem. Eng. Sci., 51 (1996) 1257–1265.
[48] M. Khayet, Membranes and theoretical modeling of membrane distillation: A review, Adv. Colloid Interface Sci., 164 (2011) 56–88.
[49] M. Ghadiri, A. Marjani, S. Shirazian, Mathematical modeling and simulation of CO_2 stripping from monoethanolamine solution using nanoporous membrane contactors, Int. J. Greenhouse Gas Control, 13 (2013) 1–8.
[50] A. Marjani, S. Shirazian, Simulation of heavy metal extraction in membrane contactors using computational fluid dynamics, Desalination, 281 (2011) 422–428.
[51] K. Tahvildari, A. Zarabpour, M. Ghadiri, A. Hemmati, Numerical simulation studies on heat and mass transfer using vacuum membrane distillation, Polym. Eng. Sci., 54 (2014) 2553–2559.
[52] M. Fasihi, S. Shirazian, A. Marjani, M. Rezakazemi, Computational fluid dynamics simulation of transport phenomena in ceramic membranes for SO_2 separation, Math. Comput. Modell., 56 (2012) 278–286.